Liquid Crystals
Publication details, including instructions for authors and subscription information:
http://www.informaworld.com/smpp/title~content=t713926090

Circular dichroism in ferroelectric and antiferroelectric liquid crystals

Ji Li[ab]; Hideo Takezoe[a]; Atsuo Fukuda[a]; Junji Watanabe[c]
[a] Department of Organic and Polymeric Materials, Tokyo Institute of Technology, Tokyo, Japan [b] Hoechst Japan Ltd., Advanced Technology Lab., Kawagoe, Japan [c] Department of Polymer Chemistry, Tokyo Institute of Technology, Tokyo, Japan

To cite this Article Li, Ji , Takezoe, Hideo , Fukuda, Atsuo and Watanabe, Junji(1995) 'Circular dichroism in ferroelectric and antiferroelectric liquid crystals', Liquid Crystals, 18: 2, 239 — 250
To link to this Article: DOI: 10.1080/02678299508036619
URL: http://dx.doi.org/10.1080/02678299508036619

LIQUID CRYSTALS, 1995, VOL. 18, NO. 2, 239–250

Circular dichroism in ferroelectric and antiferroelectric liquid crystals

by JI LI†§, HIDEO TAKEZOE*†, ATSUO FUKUDA†
and JUNJI WATANABE‡
† Department of Organic and Polymeric Materials, Tokyo Institute of Technology, O-okayama, Meguro-ku, Tokyo 152, Japan
‡ Department of Polymer Chemistry, Tokyo Institute of Technology, O-okayama, Meguro-ku, Tokyo 152, Japan

(*Received 27 May 1994; accepted 15 June 1994*)

Liquid crystal induced circular dichroism (LCICD) measurements were made to investigate the pretransitional phenomena in the S_A phase just above the S_A–S_C^* and S_A–$S_{C_A}^*$ phase transitions of both the first and the second order. The pretransitional LCICD in S_A was observed in the second order phase transition to S_C^* and $S_{C_A}^*$, suggesting the existence of a dynamic helical structure in S_A. Such behaviour disappears when the transition is of the first order. It seems that the handedness of the dynamic helix in S_A is the same as that in S_C^* even when the lower temperature phase is $S_{C_A}^*$. This is explained as a result of a dominant contribution of ferroelectric soft mode.

1. Introduction

Petransitional helical-structure formation in the isotropic (I) phase of cholesteric (Ch) liquid crystals near the I–Ch phase transition has been extensively studied by means of optical rotatory power and interpreted by the framework of Landau–de Gennes's theory [1–6]. However, only a very little has been achieved for the I phase above smectic (S) phases [4, 6]. Pretransitional helical-structure formation has also been observed in S_A above S_C^*, but only for a few materials [2, 4, 6, 7]. In these cases, the optical rotatory power in S_A has the opposite sign to that in I; this was attributed to the different nature of fluctuations in both phases.

In the cholesteric liquid crystals with high chirality, importance of the coupling of fluctuations modes was pointed out [5]. However, the experiment in the smectic liquid crystals with high chirality is scarce and the behaviour of the pretransitional rotatory power has not been clearly interpreted yet.

Recently, the antiferroelectric phase was discovered in chiral smectic liquid crystals with high chirality [8]. Interestingly, the helix handedness of the ferroelectric S_C^* and antiferroelectric $S_{C_A}^*$ phases are opposite [9]. In this sense, it is very interesting to investigate the pretransitional helical structure in the isotropic and the S_A phases of the materials which have S_C^* and/or $S_{C_A}^*$.

* Author for correspondence.
§ Present address: Hoechst Japan Ltd., Advanced Technology Lab., Minamidai 1-3-2, Kawagoe 350, Japan.

In the present work, we adopted circular dichroism (CD) measurement to investigate the pretransitional behaviour in I and S_A as well as the helical properties in S_C^* and $S_{C_A}^*$. Liquid crystal induced circular dichroism (LCICD) has extensively been studied in cholesteric liquid crystals with achiral solute [10]. The LCICD, θ, depends on (i) linear birefringence of the cholesteric (Ch) matrix, $n_Y - n_X$, (ii) linear dichroism (anisotropy of the optical density) of the solute, $OD_Y - OD_X$ and (iii) position of a selective reflection band, λ_s, relative to the absorption band, λ_{ab}. For $\lambda_{ab} < \lambda_s$, LCICD is given by

$$\tan\theta = \frac{H}{4}\frac{n_Y - n_X}{n_Y + n_X}\frac{\lambda_s}{\lambda_{ab}}\tanh(OD_Y - OD_X), \qquad (1)$$

where X and Y are taken as the short and long molecular axes in the Ch phase [11] and H ($= \pm 1$) is introduced to specify the sign due to helical handedness. Since the projection of the director is effective in the chiral smectic phases, X and Y should be taken as the directions along the P_S and C director, respectively. It should be noted that the sign of LCICD in the region of $\lambda_{ab} < \lambda_s$ depends on (i) the helical handedness and (ii) the major axis of the transition moment of the solute. Therefore, the LCICD sign provides us with characteristics of the cholesteric matrix, if characteristics of the absorption band of the solute are known. Under the condition when the transition moment is along long molecular axis, we get an LCICD which has the opposite sign to that of the CD band due to the selective reflection.

0267–8292/95 $10·00

So far, however, LCICD has never been applied for the study of pretransitional phenomena except that we recently showed the existence of LCICD in S_A [12]. The linear dichroism of the solute not only results in LCICD but also makes a contribution to the optical rotation which has strong influence on optical rotatory power. Nevertheless, the analysis of the pretransitional behaviour of the optical rotation was accomplished using de Vries equation [13] which is valid only when there is a negligible contribution from LCICD. In this context, LCICD in various phases including S_A and I is interesting.

The present work involves LCICD in I, S_A, S_C^*, $S_{C_A}^*$, $S_{C_\alpha}^*$ and $S_{C_\gamma}^*$. The $S_{C_\gamma}^*$ phase is a ferrielectric phase which is stabilized by the competition between ferroelectric and antiferroelectric interaction [14, 15], so that it may have the LCICD sign the same as that of S_C^* or of $S_{C_A}^*$ [12]. As for the $S_{C_\alpha}^*$ phase, the devil's staircase has been proposed; the structure changes stepwise and successively through various kinds of ferrielectric ordering [16–18]. The present study also includes the behaviour in S_A above both the first and the second order S_A–S_C^* and S_A–$S_{C_A}^*$ phase transition temperatures.

2. Experimental

The ferroelectric and antiferroelectric liquid crystals used in the experiments are listed in table 1 with their phase sequences and transition temperatures. All the optically pure substances listed here, except for the famous ferroelectric liquid crystal, DOBAMBC, have almost the same core structure and have high spontaneous polarizations of about $100\,nC\,cm^{-2}$. Various types of phase sequences are realized by rearranging their molecular structures [14, 15]. It should be noted that there are both substances showing the first and the second order S_A–S_C^* or S_A–$S_{C_A}^*$ phase transition.

Two kinds of homeotropic cells with high homogeneity were prepared. Thin free-standing films were made on a stainless steel plate with a small hole (3 mm in diameter), by stretching liquid crystals across over the small hole at the temperature region of S_A. Thick homeotropically aligned cells with a thickness of about 50 μm were made by coating the glass plates with surfactant AY43-021 (Toray–Dow Corning Silicone). The LCICD measurements were pursued by an automatic recording spectrometer (JASCO J20) at various temperatures controlled within $\pm$ 0·02°C. When a free-standing film cell was used, we can observe whole the LCICD signals in the fundamental absorption region. In a 50 μm thick homeotropic cell, the LCICD signal was detected only in the tail of the absorption band due to the large intrinsic absorption. The UV spectra were measured by a conventional spectrophotometer (Hitachi U3400).

Table 1. List of materials used and their phase sequences.

Samples for the investigation of the S_A–S_C^* phase transition

(1) (*R*)-MHPOOCBC

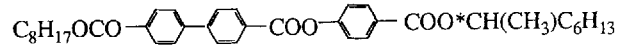

S_C^* (92·0°C) S_A (101·3°C) I

(2) (*S*)-DOBAMBC

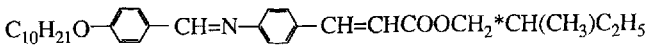

S_C^* (93·5°C) S_A (117·0°C) I

(3) (*R*:*S* = 3:1)-TFMHPDOPB [first order phase transition]

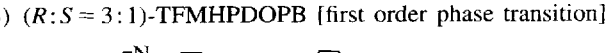

$S_{C_A}^*$ (90·0°C) S_C^* (97·0°C) S_A (105·0°C) I

Samples for the investigation of the S_A–$S_{C_A}^*$ phase transition

(4) (*R*)-TFMHPDOPB [first-order phase transition]

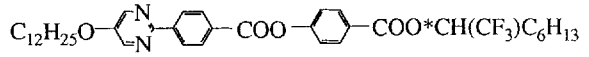

$S_{C_A}^*$ (98·0°C) S_A (105·0°C) I

(5) (*R*)-TFMHPOBC

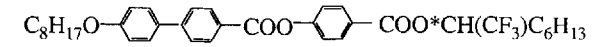

$S_{C_A}^*$ (110·0°C) S_A (120·0°C) I

(6) (*R*)-10BIMF6

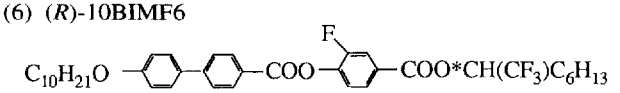

$S_{C_A}^*$ (77·0°C) S_A (97·0°C) I

(7) (*R*:*S* = 8:2)-TFMHPOBC

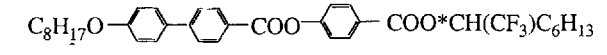

$S_{C_A}^*$ (113·0°C) S_C^* (113·5°C) S_A (124·0°C) I

Samples for the investigation of the S_A–$S_{C_\alpha}^*$ phase transition

(8) (*R*)-MHPOBC

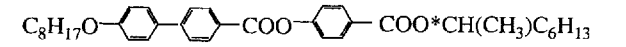

$S_{I_A}^*$ (64·0°C) $S_{C_A}^*$ (118·4°C) $S_{C_\gamma}^*$ (119·2°C)
S_C^*(120·9°C) $S_{C_\alpha}^*$ (122·0°C) S_A (148·0°C) I

(9) (*R*)-MHPOCBC

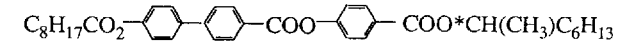

$S_{C_A}^*$ (103·5°C) $S_{C_\alpha}^*$ (122·0°C) S_A (148·0°C) I

(10) (*R*:*S* = 65:35)-MHPOCBC

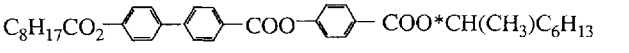

$S_{C_A}^*$ (96·0°C) S_A (148·0°C) I

3. Origin of LCICD

Before showing LCICD spectra, it is useful to discuss the origin of LCICD. First of all, an intrinsic CD of chiral molecules can be neglected compared with LCICD due to a helical structure. LCICDs are thought to be arisen from the helical formation of transition moments of the rod-like molecules of liquid crystals. Since the sign of LCICD depends not only on (i) the handedness of the helix, but also on (ii) the direction of the transition moment and on (iii) the sign of $\lambda_s - \lambda_{ab}$, it is important to know (ii) and (iii) so that we can determine the helical sense from the results of LCICD measurement.

3.1. *Transition moments*

In the present case, all the liquid crystal molecules listed in table 1 can be considered as para-disubstituted benzene, para-disubstituted biphenyl and their combinations. All of them possess long resonant structures. To consider the transition moments of such LC molecule, we start with the case of benzene.

Benzene has three absorption bands due to the π–π^* transitions. They appear at wavelengths of 183 nm, 205 nm and 255 nm, and are named B, L_a, L_b, respectively. The B band is an allowed transition which has the strongest intensity, while the L_a and L_b bands are just vibronically allowed (electronically forbidden) transitions arising from the asymmetric vibrations of the ring. Both of them lie in the plane of phenyl ring and their intensities are relatively weak [19].

Para-substituted groups have strong influences on L_a and L_b bands to cause not only a red shift but also an increase of intensity. The influence is large when one group is electron attracting and the other is electron donating or when these groups have resonant structure through the phenyl ring like the LC molecules in our case [20]. Such substitutions can change the symmetry of benzene and cause the L_a and L_b bands to be electronically allowed. In contrast to L_b, which has its transition moment perpendicular to the rod-like long molecular axis, L_a has the one parallel to the axis. So the long resonant length contributes to L_a to cause a stronger red shift in wavelength and a larger increase of intensity than to L_b. Sometimes the L_a band locates at the same or longer wavelength than the L_b band. As we can see later in almost all the samples used, λ_{L_a} is slightly longer than λ_{L_b}, although the ratio of overlapping is different due to molecular conformational difference.

In helical structures of LC, two optical eigenmodes are elliptically polarized with their axes fixed to the molecular axes and with opposite rotational senses [10]. Since L_a and L_b are attributed to the transitions whose transition moments are parallel and perpendicular to the molecular long axis, respectively, they induce the opposite signs of LCICD. In helical smectic phases, we consider the projection of L_a and L_b to the plane of smectic layer as effective parts named $L_{a(eff)}$ and $L_{b(eff)}$, respectively. Thus the intensity of $L_{a(eff)}$ strongly depends on the tilt angle while that of $L_{b(eff)}$ does not.

3.2. *Relation between λ_s and λ_{ab}*

The relation $\lambda_{ab} < \lambda_s$ must be valid to use equation (1). There is no problem in the helical phases such as S_C^* and $S_{C_A}^*$ according to the previous pitch measurements [21].

We have to infer the pitch of dynamic helix formed in the S_A phase for the application of equation (1) to this phase. In the case of second order S_A–S_C^* phase transition, it is reasonable to consider that the helical fluctuation in S_A reflects the symmetry of S_C^*. In high temperature region of S_A, there exists a helical fluctuation with very short correlation length. With the decrease of temperature, the correlation length becomes longer. At the same time the distribution of pitch becomes sharp. When temperature decreases to the S_A–S_C^* transition point, the correlation length grows infinitely to cause 'freezing of soft mode' together with convergence of the distributed pitch to a certain value P_0, the pitch of S_C^* phase at the transition point. Thus the pitch of dynamic helix at the transition point can be considered to be the same as that of the static helix of S_C^* phase at the transition point.

The existence of dynamic helix is observed in S_A above $S_{C_A}^*$, though it is not the case for the first order S_A–$S_{C_A}^*$ transition. The same argument is valid in S_A above $S_{C_A}^*$, though the transition is sometimes weakly first order. So in this sense, leaving some other possibilities, it is reasonable to assume that the change in pitch at the transition point is almost continuous. Thus, the relation $\lambda_{ab} < \lambda_s$ is valid in all phases of all the liquid crystals used in the present study, except for $S_{C_\alpha}^*$, whose helical structure is unknown.

4. Results and discussion

4.1. *Two absorption bands and their LCICD*

Before showing LCICD of individual compounds, it is useful to see the typical LCICD due to $L_{a(eff)}$ and $L_{b(eff)}$ together with the absorption spectrum. Figure 1 (*a*) shows the UV spectrum of (*R*)-TFMHPDOPB dissolved in ethanol. There is a peak at the wavelength of 290 nm and a shoulder of this peak in the longer wavelength region. The peak and the shoulder can be attributed to L_a and L_b, respectively. It is difficult to clearly separate L_b from L_a, since both of them are broad and are largely overlapped.

In contrast to the UV spectrum, the CD spectrum in figure 1 (*b*) elucidates the two bands more clearly. The measurement was pursued at the temperature range of $S_{C_A}^*$ in a free-standing film. The peak at the wavelength of 480 nm with a minus sign is due to the selective reflection and the other two peaks with opposite signs in the shorter

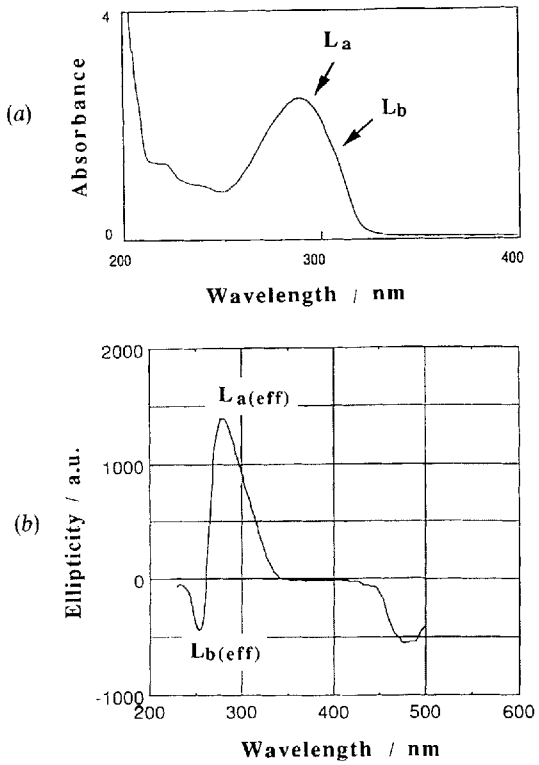

Figure 1. (*a*) UV absorption spectrum of (*R*)-TFMHPDOPB in ethanol and (*b*) CD spectrum of (*R*)-TFMHPDOPB in a free-standing film. Since the $L_{a(eff)}$ and $L_{b(eff)}$ bands have transition moments perpendicular to each other, and thus induce LCICDs with opposite signs, they appear more clearly in the CD spectrum than in the UV spectrum. The negative CD peak at 480 nm in (*b*) is due to the selective reflection.

wavelength region are LCICDs. Although they are partially overlapped, we can easily determine $L_{a(eff)}$ and $L_{b(eff)}$, as illustrated in figure 1 (*b*), based on the relative intensities and the signs. The difference in the relative position of L_a (or $L_{a(eff)}$) and L_b (or $L_{b(eff)}$) in figures 1 (*a*) and (*b*) manifests the sensitiveness of the wavelength.

It should be noted that $L_{b(eff)}$ is hidden and $L_{a(eff)}$ is dominantly observed, if the two bands overlap completely and the tilt angle in S_C^* or $S_{C_A}^*$ phase is relatively large, as in the case of figure 1 (*b*). If the measurement is carried out at the temperature where the tilt angle is small, the $L_{a(eff)}$ becomes very weak and we can rather observe $L_{b(eff)}$ dominantly.

Figure 2 shows a temperature dependence of absorbance at 350 nm of (*R*)-MHPOBC in a homeotropically aligned thick cell. In the isotropic phase, both $L_{a(eff)}$ and $L_{b(eff)}$ contribute to the absorption, while $L_{a(eff)}$ becomes very small and $L_{b(eff)}$ gives major contribution on LCICD in S_A because of the homeotropic alignment. A strong absorption in I indicates that $L_{a(eff)}$ has higher oscillator strength than $L_{b(eff)}$. Considerable absorption in S_A and very small temperature dependence in S_C^* compared with that of the director tilt angle suggest fairly large contribution of $L_{b(eff)}$ to the absorption.

4.2. *LCICD spectra in helical phases*

Figures 3, 4 and 5 show LCICD spectra of eight substances; figure 3 for (1) (*S*)-DOBAMBC, (2) (*R*)-MHPOOCBC and (3) (*R*:*S* = 3:1) TFMHPDOPB with the S_A–S_C^* phase transition, figure 4 for (4) (*R*)-TFMHPDOPB, (5) (*R*)-TFMHPOBC and (6) (*R*)-10BIMF6 with the S_A–$S_{C_A}^*$ phase transition and figure 5 for (7) (*R*)-MHPOBC and (8) (*R*)-MHPOCBC with the S_A–$S_{C_z}^*$ phase transition. The upper and lower parts show spectra of normal cells and free-standing films, respectively. In the spectra for free-standing cells, strong LCICD peak can be seen in S_C^* or $S_{C_A}^*$ in a short wavelength region near 300 nm, while, in those for normal cells, LCICD is observed only in the absorption tail. A strong $L_{a(eff)}$ peak and a weak $L_{b(eff)}$ peak with the opposite sign to the $L_{a(eff)}$s can be seen in the S_C^* or $S_{C_A}^*$ phase of most of the materials. The existence of the $L_{b(eff)}$ peak is clear particularly in figures 3 (*c'*), 4 (*a'*) and 4 (*b'*), suggesting that a CF_3 group perpendicular to the long axis of liquid crystal molecules has stronger contribution to $L_{b(eff)}$ than a CH_3 group.

In the S_A phase, the LCICD signal in the free-standing films is difficult to be detected because of lack of film thickness, except DOBAMBC and MHPOOCBC showing a typical second order S_A–S_C^* transition. For DOBAMBC, the $L_{a(eff)}$ becomes smaller and smaller with increasing temperature from S_C^* to S_A (see figure 3 (*a'*) spectra

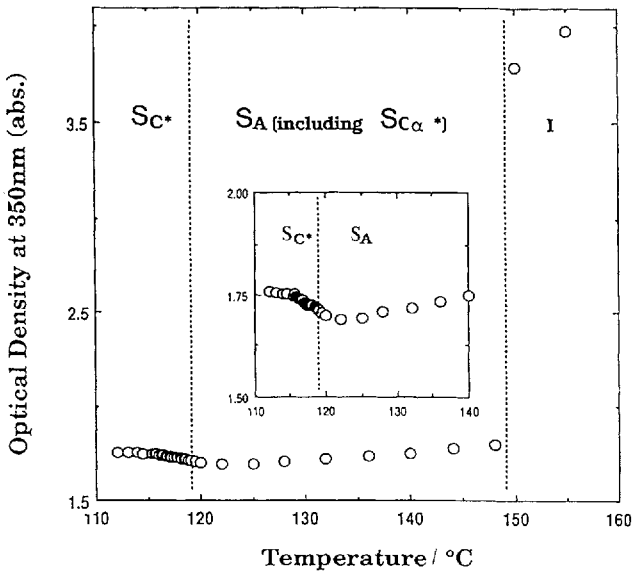

Figure 2. Temperature dependence of absorbance at 350 nm of (*R*)-MHPOBC in a 50 μm-thick homeotropic cell. The $L_{b(eff)}$ band gives major contribution to the absorption except in S_A. In the S_C^* phase, the change of absorbance reflects the change of the tilt angle of the LC molecules.

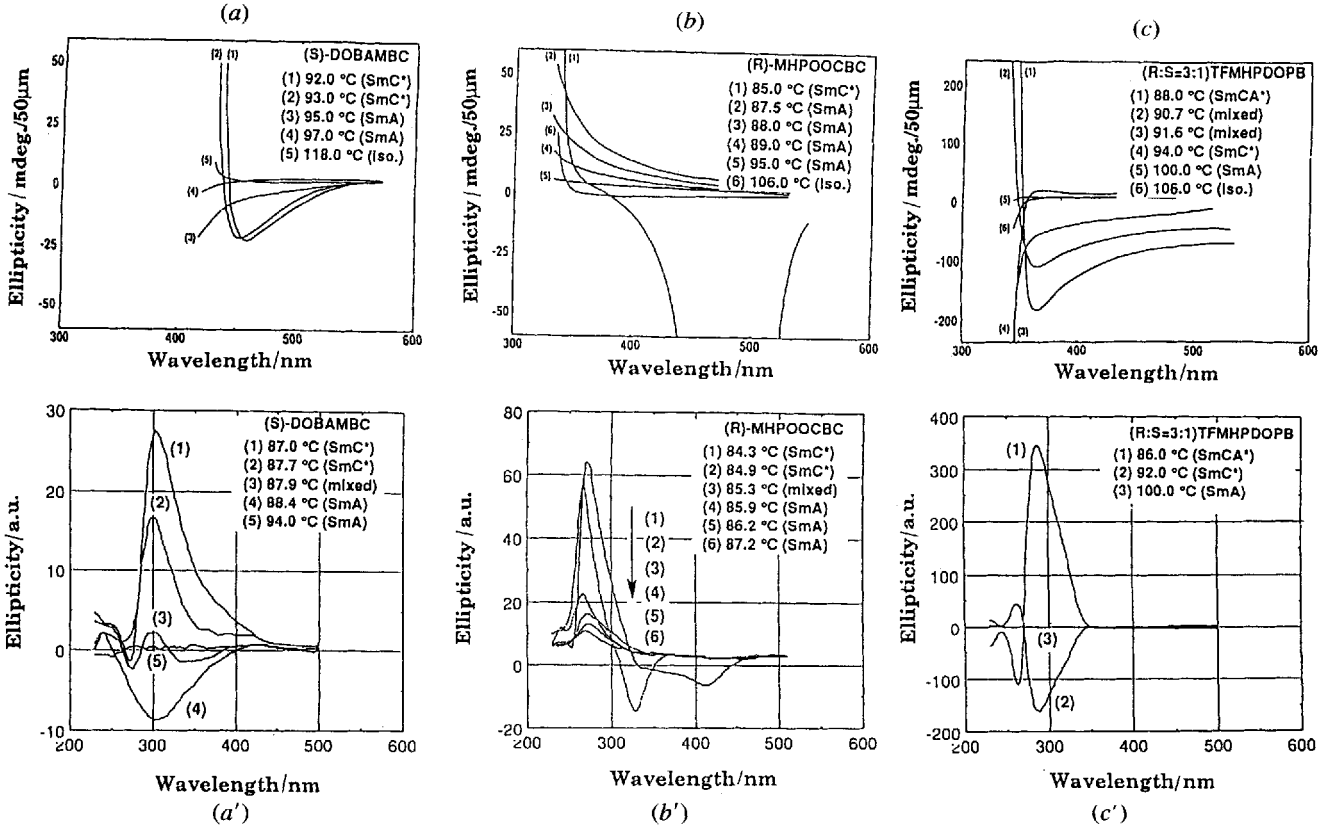

Figure 3. CD spectra of substances with the S_A–S_C^* phase transition. The upper part, (*a*), (*b*) and (*c*), and the lower part (*a'*), (*b'*) and (*c'*), show spectra of 50 μm thick cells and free standing films, respectively. The substances, (*S*)-DOBAMBC and (*S*)-MHPOOCBC, show the second-order S_A–S_C^* phase transition and the third one, (*R*:*S* = 3:1)-TFMHPDOPB shows the typical first order S_A–S_C^* phase transition. In addition to LCICDs, the CDs due to the selective reflection of S_C^* helix appear in the longer wavelength region in (*b*) and (*b'*) with the opposite sign to the corresponding LCICDs of $L_{a(eff)}$.

(1)–(3)), and finally only $L_{b(eff)}$ can be observed (see figure 3 (*a'*) spectrum (4)). Thus, the opposite LCICD sign in the S_A and S_C^* phases of DOBAMBC is seen. The observation is explained by the change in the contribution of $L_{a(eff)}$ and $L_{b(eff)}$ associated with the temperature dependence of the tilt angle; the contribution of $L_{b(eff)}$ is dominant in the S_A phase and that of $L_{a(eff)}$ increases with decreasing temperature, namely with increasing tilt angle, in the S_C^* phase. Since $L_{a(eff)}$ and $L_{b(eff)}$ give the opposite sign of LCICD as mentioned above, the sign change of LCICD occurs. The spectrum of MHPOOCBC, however, shows rather an $L_{a(eff)}$ contribution in the S_A phase. The differences of the transition moment in their strength and direction between DOBAMBC and MHPOOCBC, arising from the different resonant structure, may result in such different spectra.

To catch the weak LCICD signal in each phase, we show experimental results of thick cells in figures 3 (*a*), (*b*), (*c*), 4 (*a*), (*b*), (*c*), 5 (*a*) and (*b*). Although we can detect only the tail of the LCICD signal, much information which cannot be seen from the spectra of free-standing films is involved in these spectra. Not only sharp rises in the helical phases such as S_C^* and $S_{C_A}^*$ but also increases of LCICD in non-helical phases such as S_A and I are observed. The latter LCICDs, though not large, are due to the pretransitional formation of helical structure.

In figures 3 (*b*), (*b'*), 4 (*a*), (*a'*), (*b*) and 5 (*a*), we can also see the CD signals of selective reflections at longer wavelength. It is clear that the CD of selective reflection has the opposite sign to the LCICD of $L_{a(eff)}$. This observation is consistent with the fact that the transition of $L_{a(eff)}$ lies in the direction of long axis of the rod like LC molecules.

From the spectra of thick cells, we can also observe remarkable features in LCICD spectra in helical phases; with decreasing wavelength, LCICD spectra show a dip before sharp rise. It is considered to be the contribution of $L_{b(eff)}$ which seems to have a wider band width as seen in figure 3 (*a'*). Such feature is more frequently seen in $S_{C_A}^*$ phase. Actually, in (*R*:*S* = 3:1)-TFMHPDOPB (see figure 3 (*c*)), the dip disappears when the $S_{C_A}^*$–S_C^* phase transition occurs. The different positional relation in the wavelengths of $L_{a(eff)}$ and $L_{b(eff)}$ in S_C^* and $S_{C_A}^*$ may cause the difference.

As for the sign of LCICD, two findings should be made.

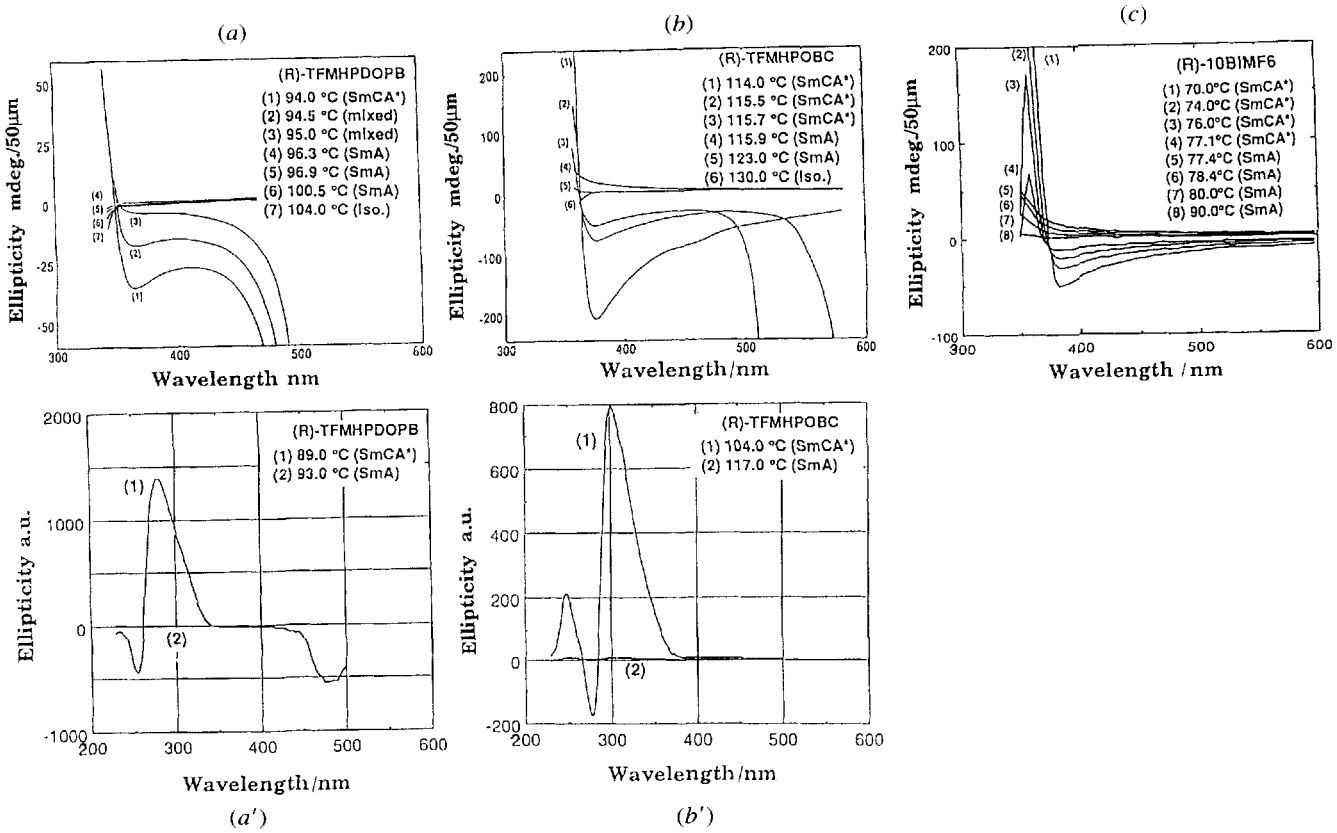

Figure 4. CD spectra of substances with the S_A–$S^*_{C_A}$ phase transition. The upper part, (*a*), (*b*) and (*c*), and the lower part, (*a'*) and (*b'*), show spectra of 50 μm thick cells and free standing films, respectively. (*R*)-TFMHPDOPB shows the typical first order S_A–$S^*_{C_A}$ phase transition and its spectrum is similar to that of (*R*:*S* = 3:1)-TFMHPDOPB shown in figures 3 (*c*) and (*c'*). The spectra of (*b*) (*R*)-TFMHPOBC and (*c*) (*R*)-10BIMF6 have a similar trend in its temperature dependence. Both of them show the second order S_A–$S^*_{C_A}$ phase transition. The CDs of selective reflection can also be seen in (*a*), (*a'*) and (*b*).

First, the sign in I is always the same as that in S^*_C and opposite to that in $S^*_{C_A}$. Secondly, the signs in I and S_A are the same in most of the cases with the exceptions of DOBAMBC and TFMHPOBC. Demikhov *et al.* [7], explained an anomalous sign change of optical rotation in S_A and I of DOBAMBC as the results of different structure of orientational fluctuation between these two phases by using Landau's theory. In our LCICD experiment in DOBAMBC, we just simply interpret such exception as the different contributions of $L_{a(eff)}$ or $L_{b(eff)}$ transition moment as mentioned above. For TFMHPOBC and 10BIMF6, different signs in S_A from the signs in I are found and will be discussed later.

Based on the interpretations and discussions about the spectra, we list the signs of LCICD with the contributing transition moments in table 2.

4.3. *Pretransitional phenomena*

In figures 6, 7 and 8 are shown LCICDs in the long wavelength tail of the fundamental absorption band. It is noted that pretransitional LCICD is observed in S_A as well as in I. As mentioned in § 1, pretransitional formation of helix in S_A is less studied compared with that in I. Therefore, our main attention is paid to S_A above S^*_C and $S^*_{C_A}$ including the first order phase transition.

4.3.1. *S_A–S^*_C phase transition*

Let us show in figures 6 (*a*)–(*c*) such pretransitional behaviour in the S_A phase above the S_A–S^*_C transition point. Both (*S*)-DOBAMBC and (*R*)-MHPOOCBC shown in figures 6 (*a*) and (*b*) are materials showing the second order S_A–S^*_C phase transition. The main difference between them is their spontaneous polarizations. (*R*)-MHPOOCBC has a large P_s near 100 nC cm^{-2} while (*S*)-DOBAMBC has a P_s of 4 nC cm^{-2}. In contrast to the above materials, the third substance, (*R*:*S* = 3:1)-TFMHPDOPB, shown in figure 6 (*c*) exhibits a typical first order S_A–S^*_C phase transition [9, 22].

As clearly shown in figures 6 (*a*) and (*b*), LCICD increases with decreasing temperature and approaching to the second order transition point, indicating the existence of pretransitional phenomenon in the S_A phase, namely the formation of dynamic helical structure in the S_A phase in the vicinity of the transition point. Short range S^*_C order

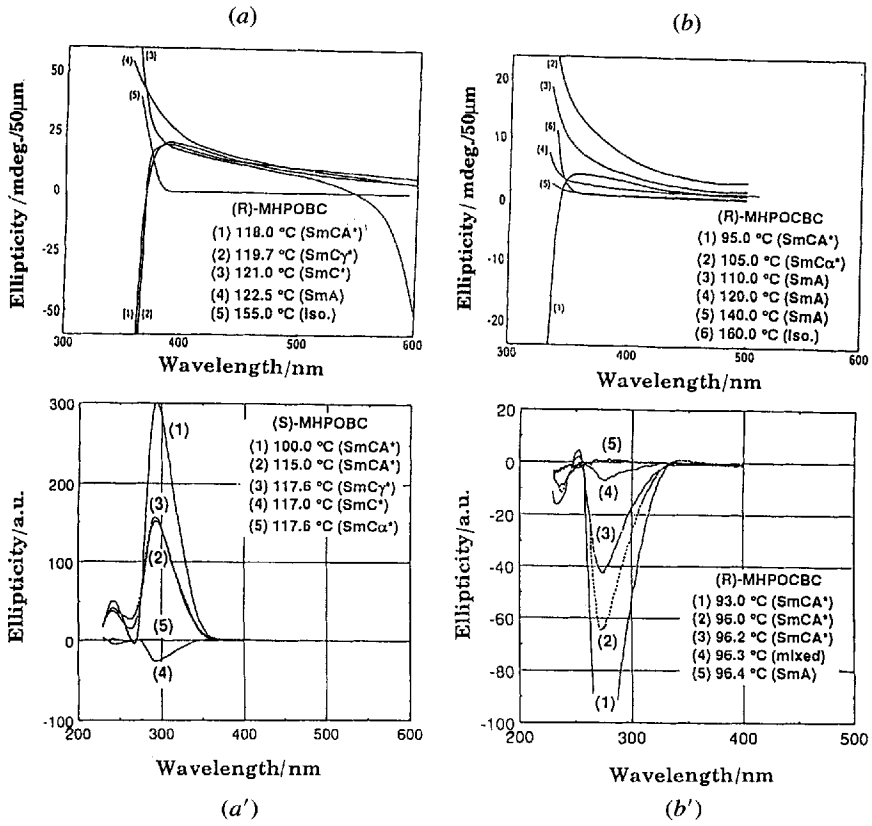

Figure 5. CD spectra of substances, (*R*)-MHPOBC and (*R*)-MHPOCBC, with the S_A–$S^*_{C\alpha}$ phase transition. The upper part, (*a*) and (*b*), and the lower part, (*a'*) and (*b'*), show spectra of 50 μm thick cells and free standing films, respectively. $S^*_{C\alpha}$ shows weaker LCICD than S_A.

Table 2. LCICD sign in various phases together with major contribution, $L_{a(eff)}$ or $L_{b(eff)}$.

	Phase						
Substance	I	S_A	$S^*_{C\alpha}$	S^*_C	AF*	$S^*_{C\gamma}$	S^*_{CA}
(*S*)-DOBAMBC	+ (L_a)	− (L_b)		+ (L_a)			
(*R*)-MHPOOCBC	+ (L_a)	+ ($L_{a?}$)		+ (L_a)			
(*R*:*S* = 3:1) TRFMHPDOPB	+ (L_a)	0		+ (L_a)			− (L_a)
(*R*)-TFMHPDOPB	+ (L_a)	0					− (L_a)
(*S*)-TMFHPOBC	+ (L_a)	− (L_b)					− (L_a)
(*R*:*S* = 2:8) TFMHPOBC	+ (L_a)	− (L_b)		+ (L_a)			− (L_a)
(*S*)-TFMNPOBC	+ (L_a)	− ($L_{b?}$)					− (L_a)
(*S*)-10BIMF6	+ (L_a)	− (L_b)					− (L_a)
(*R*)-MHOPBC	+ (L_a)	+ ($L_{b?}$)	+ ($L_{b?}$)	+ (L_a)		− (L_a)	− (L_a)
(*R*)-MHPOCBC	+ (L_a)	+ ($L_{b?}$)	+ ($L_{b?}$)				− (L_a)
(*R*:*S* = 65:35) MHPOCBC	+ (L_a)	+ ($L_{b?}$)					− (L_a)

appears dynamically over a certain correlation length. When temperature decreases to the vicinity of the S_A–S^*_C transition point, the correlation length grows, causing an increase of the LCICD signal.

According to Battle *et al.* [5], the effect of coupling between chiral modes, which is not seen in DOBAMBC, should appear both in the isotropic and S_A phases to make up a maximum of optical rotatory power in the temperature range near the transition point, if the chirality is sufficiently high. It is noticed, however, that the LCICD intensities of the pretransitional effect in both materials are almost of the same order, suggesting that the spontaneous polarization has little influence on the pretransitional behaviour in the S_A phase.

According to the relation between the sign of LCICD and the handedness of the helix, the dynamic helical structures in the pretransitional region of S_A just above the second order S_A–S^*_C phase transition have the same sense as that in the S^*_C phase. For the material showing the first order S_A–S^*_C phase transition, the result is completely

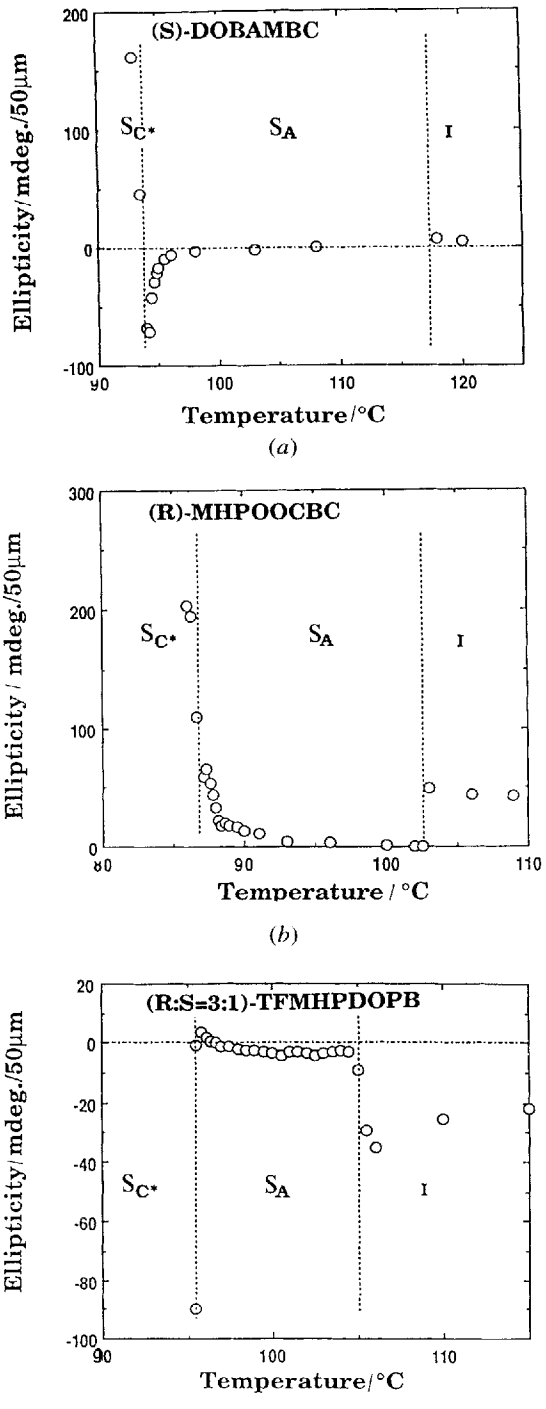

Figure 6. Temperature dependence of LCICD intensity measured at the wavelength of 432 nm for (*a*) (*S*)-DOBAMBC, 337 nm for (*b*) (*R*)-MHPOOCBC and 346 nm for (*c*) (*R*:*S* = 3:1)-TFMHPDOPB, all of which show the S_A–S_C^* phase transition. Pretransitional phenomenon in S_A phase can be observed in (*a*) (*S*)-DOBAMBC and (*b*) (*R*)-MHPOOCBC whose S_A–S_C^* phase transition is of the second order but cannot in (*c*) (*R*:*S* = 3:1)-TFMHPDOPB with the typical first order S_A–S_C^* phase transition.

different. The pretransitional behaviour in the S_A phase can hardly be seen when the S_A–S_C^* transition is of the first order, as shown in figure 6 (*c*).

In the case of the pretransitional behaviour in the isotropic phase of the cholesteric liquid crystal, Yang measured the dynamic Ch-like pitch in I near the transition point using the Bragg scattering technique [23]. In our case, however, the determination of the S_C^*-like pitch of the dynamic helix is difficult, even if the pitch length is suitable for the scattering technique, because the tilt angle may be too small to make a clear periodical change of refractive index.

4.3.2. S_A–$S_{C_A}^*$ *phase transition*

Figure 7 shows results for three samples with the S_A–$S_{C_A}^*$ phase transition. (*R*)-TFMHPDOPB has a typical first order S_A–$S_{C_A}^*$ phase transition accompanied by a sudden structure change [22], while (*R*)-TFMHPOBC and (*R*)-10BIMF6 have transitions of the quasi-second or weakly first order [24]. Their structural changes in helix and layer tilt near the phase transition temperature have been investigated by using the selective reflection method and the X-ray diffraction [9, 24, 25].

The result shown in figure 7 (*a*) indicates that, similar to the case of (*R*:*S* = 3:1)-TFMHPDOPB mentioned in § 4.3.1, the pretransitional behaviour does not exist. This is a natural consequence in the first order phase transition. A pretransitional behaviour is detected in (*R*)-TFMHPOBC and (*R*)-10BIMF6, as shown in figures 7 (*b*) and (*c*). Since the transition is of the quasi-second order, the change of LCICD intensity at the transition point is not so smooth as the case of a typical second order phase transition.

It is noted in figures 7 (*b*) and (*c*) that the LCICD sign in S_A is the same as that in the $S_{C_A}^*$ phase. However, from the temperature dependences of the LCICD spectra, particularly in the case of (*R*)-10BIMF6 (see figure 4 (*c*)), we can judge that the LCICD due to $L_{b(eff)}$ reverses its sign at the transition point. Thus the LCICD in S_A and $S_{C_A}^*$ plotted in figures 7 (*b*) and (*c*) are due to different contributions of transition moments, i.e. $L_{a(eff)}$ in $S_{C_A}^*$ and $L_{b(eff)}$ in S_A (see table 2). This fact suggests the possibility that the handedness of dynamic helix in S_A may be opposite to that in $S_{C_A}^*$, namely the same as that in S_C^*. We can imagine that the dynamic helix in S_A just above $S_{C_A}^*$ is S_C^* like, as will be discussed later.

4.3.3. S_A–$S_{C_2}^*$ *phase transition*

In figures 5 and 8, we can see that the pretransitional phenomenon is also observed in S_A above the S_A–$S_{C_2}^*$ transition. The LCICD sign in $S_{C_2}^*$ seems to be always the same as that in S_C^*, but since the types of materials are limited and the structure of $S_{C_2}^*$ is not clarified till now, it is difficult to determine whether the pretransitional

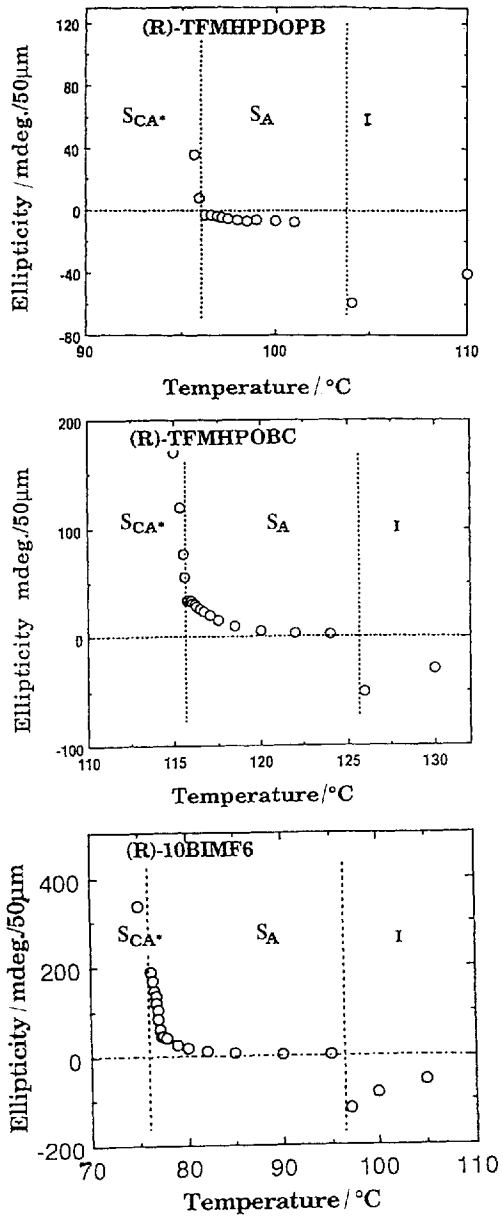

Figure 7. Temperature dependence of LCICD intensity measured at the wavelength of 347 nm for (*a*) (*R*)-TFMHPDOPB, 365 nm for (*b*) (*R*)-TFMHPOBC and 367 nm for (*c*) (*R*)-10BIMF6, all of which show the S_A–$S^*_{C_A}$ phase transition. Similar to the case in figure 6, pretransitional phenomenon in S_A is detected only in (*b*) (*R*)-TFMHPOBC and (*c*) (*R*)-10BIMF6 with the second or quasi-second order S_A–$S^*_{C_A}$ phase transition.

phenomenon is S^*_C-like, $S^*_{C_A}$-like or $S^*_{C_\alpha}$-like at present time.

4.3.4. *Dominant soft mode in S_A*

It is very interesting to consider what kind of dynamic helix is formed in the S_A phase. By properly taking account of the sign of LCICD in S_A together with the main contribution of $L_{a(eff)}$ and $L_{b(eff)}$ bands on LCICD, we suggested above that the dynamic helix is S^*_C like even when the lower temperature phase is $S^*_{C_A}$ or $S^*_{C_\alpha}$.

In order to consider the possibility for the occurrence, let us discuss the soft mode in the S_A phase. It has been reported by various authors that in ferroelectric liquid crystals there exist ferroelectric soft mode (FSM) in the S_A phase and ferroelectric Goldstone mode (FGM) in the S^*_C phase [26, 27]. Recently, antiferroelectric liquid crystals were discovered and possibilities of the existence of antiferroelectric soft (AFSM) mode and antiferroelectric Goldstone mode (AFGM) were pointed out [28]. Here we consider the relaxation of these soft modes near the S_A–S^*_C (or S_A–$S^*_{C_A}$) transition point. For simplicity, we only consider the relaxation time of the modes that have their

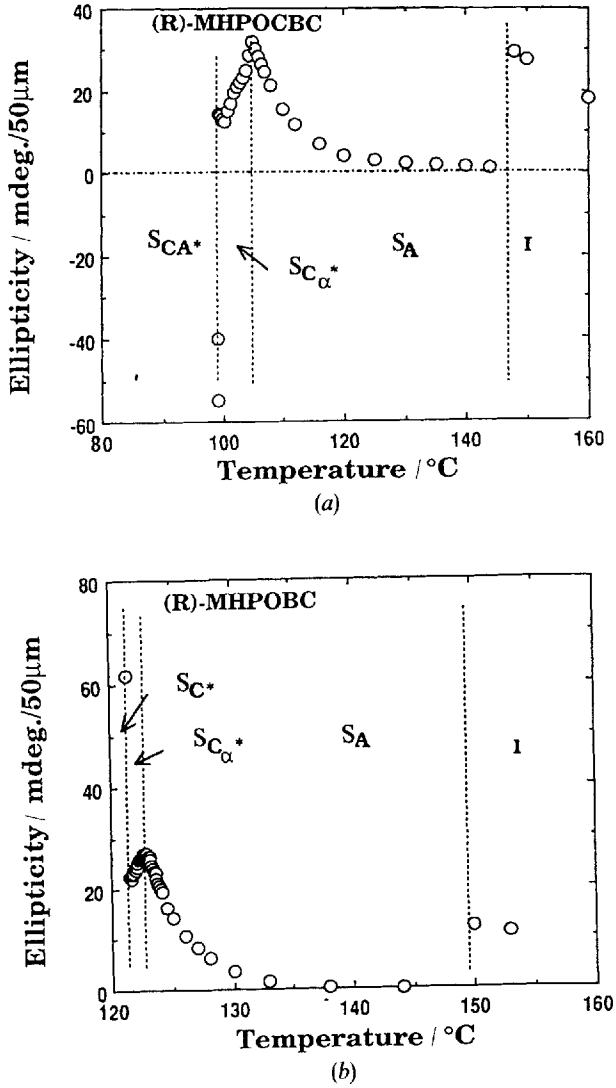

Figure 8. Temperature dependence of LCICD intensity measured at the wavelength of 340 nm for (a) (*R*)-MHPOCBC and 360 nm for (*b*) (*R*)-MHPOBC, both of which show the S_A–$S^*_{C_\alpha}$ phase transition.

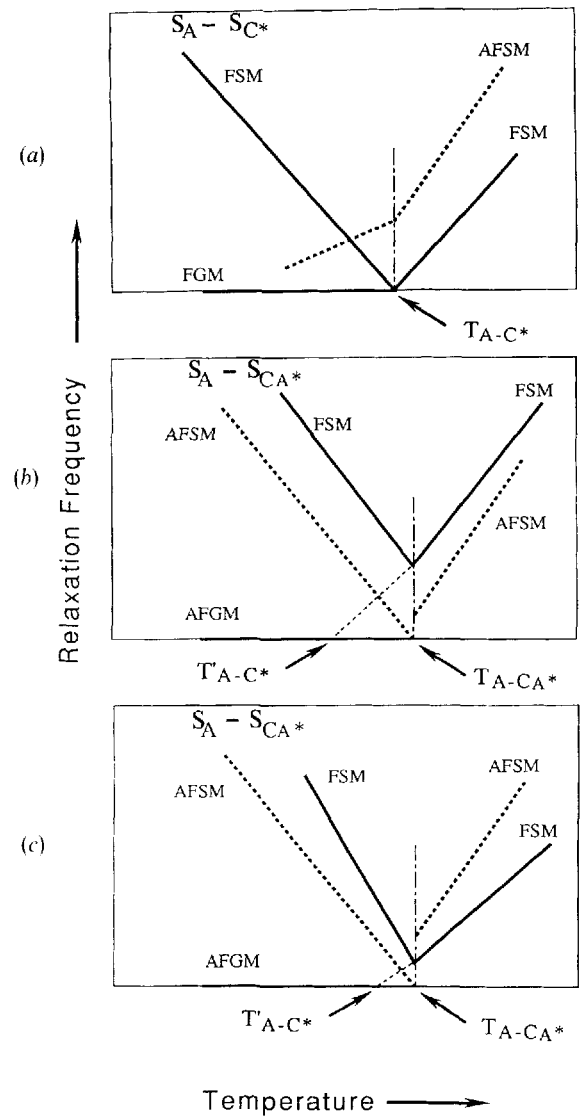

Figure 9. Illustration of relaxation frequency of ferroelectric soft mode (FSM), ferroelectric Goldstone mode (FGM), antiferroelectric soft mode (AFSM) and antiferroelectric Goldstone mode (AFGM). There exist three possible cases. In cases of (*a*) and (*b*), the phases with the soft mode of lower frequency appears as the lower temperature helical phases, while the $S^*_{C_A}$ phase appears as a result of the first order phase transitions in the case (*c*), although FSM has lower frequency in S_A.

wavevector $K = K_0$, where K_0 refers to the wavevector of S^*_C or $S^*_{C_A}$ helix at the transition point.

In S_A of antiferroelectric liquid crystals, there should exist both FSM and AFSM as shown in figure 9 (*a*). With decreasing temperature, the two soft modes become soft. If the phase below S_A is S^*_C, the relaxation frequency of FSM is lower than that of AFSM and it decreases to zero at the S_A–S^*_C transition point, $T_{S_A\text{-}S^*_C}$ (see figure 9 (*a*)). If the lower temperature phase is $S^*_{C_A}$, the frequency of AFSM is lower than that of FSM and decreases toward the S_A–$S^*_{C_A}$ transition point (see figure 9 (*b*)). In this case the FSM is considered to become soft toward $T'_{S_A\text{-}S^*_C}$ which is lower than $T_{S_A\text{-}S^*_{C_A}}$, although the S^*_C phase does not appear because of the emergence of $S^*_{C_A}$. The small frequency jump of AFSM at the S_A–$S^*_{C_A}$ transition point is drawn according to the fact that till now almost all S_A–$S^*_{C_A}$ is somewhat of the first order with a small jump in its structure change.

In figures 9 (*a*) and (*b*), the soft mode with lower relaxation frequency is stabilized to realize the S^*_C or $S^*_{C_A}$ phase on low temperature side, respectively. Because of the structure jump at the S_A–$S^*_{C_A}$ transition point, there also exists the third possibility as illustrated in figure 9 (*c*). In this case, although the transition is S_A–$S^*_{C_A}$, the soft mode with lower relaxation frequency in S_A can be FSM.

The diagram shown in figure 9 (*c*) explains the sign of dynamic helix in S_A to be different from that of static helix

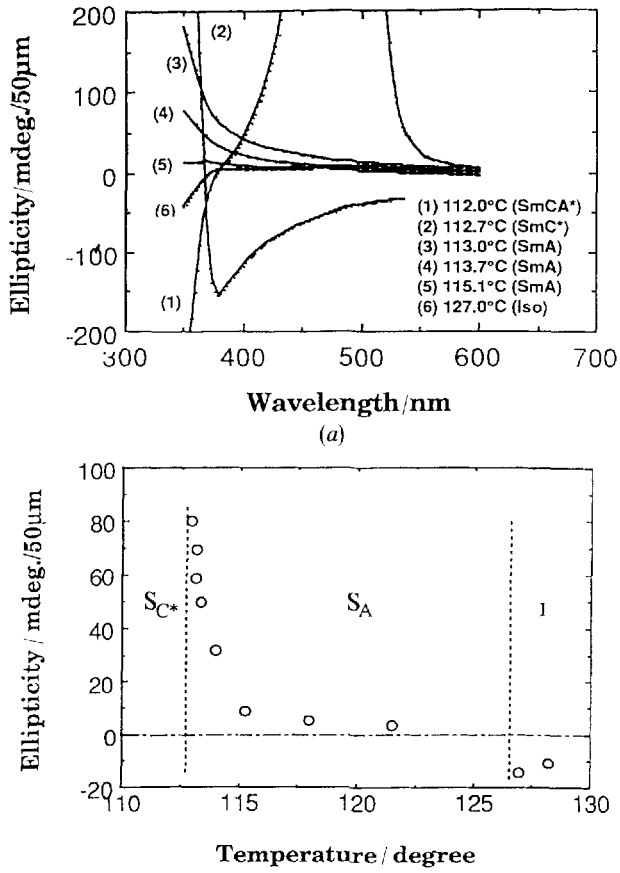

Figure 10. CD spectra and temperature dependence of LCICD intensity of (*R*:*S* = 8:2)-TFMHPOBC measured at the wavelength of 365 nm. By comparing these figures with figure 4 (*b*) and figure 7 (*b*), the appearance of S^*_C by the reduction of optical purity has little influence on the pretransitional phenomenon in S_A.

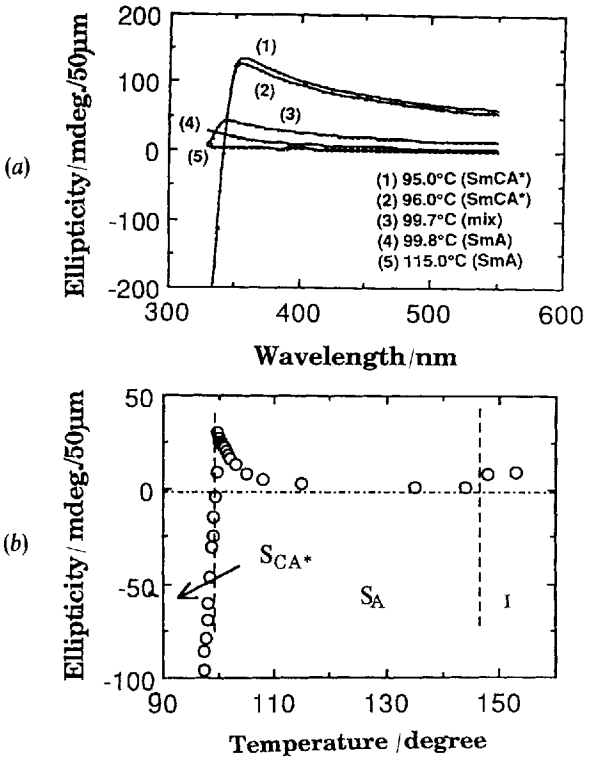

Figure 11. CD spectra and temperature dependence of LCICD intensity of $(R:S = 65:35)$-MHPOCBC measuring at 365 nm. By comparing these figures with figures 5 (*b*) and 8 (*a*), the disappearance of $S^*_{C_\alpha}$ by the reduction of optical purity has little influence on the pretransitional phenomenon in S_A.

Table 3. The dominant soft modes in the S_A phase of each substance with the phase sequences. The mark '0' in the table refers to the case when there exists no pretransitional phenomenon. FSM is the dominant fluctuations in the cases of the second order S_A–S^*_C phase transitions. In those with the S_A–$S^*_{C_A}$ phase transitions, the results show that the dominant soft mode is FSM, although there exist some uncertainties due to some experimental difficulties. For the S_A–$S^*_{C_\alpha}$ transition, the judgement is impossible for lack of structural information of $S^*_{C_\alpha}$ at the present stage.

Substance	Dominant soft mode in S_A phase	Phase sequence
(*S*)-DOBAMBC	FSM	S_A–S^*_C
(*R*)-MHPOOCBC	FSM	S_A–S^*_C
$(R:S = 3:1)$ TFMHPDOPB	0	S_A–S^*_C–$S^*_{C_A}$
(*R*)-TFMHPDOPD	0	S_A–$S^*_{C_A}$
(*S*)-TFMHPOBC	FSM (? AFSM)	S_A–$S^*_{C_A}$
$(R:S = 2:8)$ TFMHPOBC	FSM (? AFSM)	S_A–S^*_C–$S^*_{C_A}$
(*S*)-TFMNPOBC	FSM (? AFSM)	S_A–$S^*_{C_A}$
(*S*)-10BIMF6	FSM (? AFSM)	S_A–$S^*_{C_A}$
(*R*)-MHPOBC	?	S_A–$S^*_{C_\alpha}$–S^*_C
(*R*)-MHPOCBC	?	S_A–$S^*_{C_\alpha}$–$S^*_{C_A}$
$(R:S = 65:35)$ MHPOCBC	?	S_A–$S^*_{C_A}$

in $S^*_{C_A}$ as described in § 3.1. The existence of the hidden S^*_C phase near the S_A–$S^*_{C_A}$ transition point can easily be confirmed by slightly reducing the optical purity of TFMHPOBC [29]. We show the CD spectrum and the temperature dependence of LCICD of $(R:S = 8:2)$-TFMHPOBC in figures 10 (*a*) and (*b*). The comparison of these with that of (*R*)-TFMHPOBC (see figures 4 (*b*) and 7 (*b*)) shows that the appearance of S^*_C has little inference on pretransitional behaviour. All these results inferred that TFMHPOBC is just the case shown in figure 9 (*c*) and its dynamic helix is S^*_C-like (FSM).

Such phenomenon can even be seen when we eliminate the $S^*_{C_\alpha}$ phase by reducing the optical purity. One example for $(R:S = 8:2)$-MHPOCBC is shown in figure 11. We can see by comparing figures 5 (*b*), 8 (*a*) and 11, that the elimination of $S^*_{C_\alpha}$ has little inference on pretransitional behaviour.

A similar phenomenon is also observed in the pretransitional behaviour in I which is not affected by the S_A–$S^*_{C_A}$ or S_A–S^*_C phase transition. We suppose that the pretransitional behaviour in I depends on the I–Ch phase transition to appear or to be expected to appear on the low temperature side. If there exists the Ch phase in the materials used in the present study, the sign of LCICD of Ch will be the same as that in the S^*_C phase. Thus, the sign of LCICD in I is the same as that in the S^*_C phase.

In table 3 is summarized the dominant soft mode in the S_A phase based on the above discussion. The pretransitional fluctuation is only observed in S_A when the phase transition is of the second or quasi-second order. It is reasonable that the soft mode in S_A just above the S_A–S^*_C transition point of a ferroelectric liquid crystal is FSM. As for the case of antiferroelectric liquid crystal, the situation is more complicated because the existence of S^*_C, really or potentially, is thought to affect the results. Since the materials possessing $S^*_{C_A}$ used in our experiments usually have such S^*_C, really or potentially, the dominant soft mode is determined to be FSM, although the other possibility cannot be excluded completely for the difficulties of experiments. The possibility should also be noted that, with the development of materials with strong antiferroelectricity, the ferroelectric S^*_C phase is strongly suppressed so that the dominant soft mode in S_A above the S_A–$S^*_{C_A}$ transition point can be AFSM. For the compounds with $S^*_{C_\alpha}$, the clarification of the unknown structure of this phase will be a key point to elucidate the soft mode in the S_A phase.

5. Conclusion

Application of LCICD measurement provides much information on both static and dynamic helical structures of ferroelectric and antiferroelectric liquid crystals. By detecting the LCICD in the intrinsic absorption band, we found pretransitional phenomena in the S_A phase towards

S_A–S_C^* or S_A–$S_{C_A}^*$ transition point, if the transition is of the second-order. This is explained by the formation of the dynamic helical structure. When the transition is of the first order, such phenomenon is not observed. Most of the data show that the handedness of dynamic helix in the pretransitional regime of the S_A phase is the same as that in S_C^* for the existence or potential existence of this phase. To confirm these results further studies with a wide variety of materials are necessary.

Showa Shell Sekiyu K.K., Kashima Oil Co., Ltd. and Mitsubishi Chemical Co., Ltd. are gratefully acknowledged for supplying liquid crystals. This work was partly supported by a Grant-in-Aid for Scientific Research (No. 04452089 and No. 06102005) from the Ministry of Education, Science and Culture.

References

[1] DE GENNES, P. G., 1971, *Molec. Crystals liq. Crystals.*, **12,** 193. (a) CHENG, J., and MEYER, R. B., 1974, *Phys. Rev.* A, **9,** 2744.
[2] BRAZIVSKII, S. A., and DMITRIEV, S. G., 1976, *Soviet Phys. JETP*, **42,** 497.
[3] DOLGANOV, V. K., KRYLOVA, S. P., and FILEV, V. M., 1980, *Soviet Phys. JETP.*, **51,** 1177.
[4] FILEV, V. M., 1983, *Soviet Phys. JETP Lett.*, **37,** 703.
[5] BATTLE, P. R., MILLER, J. D., and COLLINGS, P. J., 1987, *Phys. Rev.* A, **36,** 369.
[6] FRAME, K. C., WALKER, J. L., and COLLINGS, P. J., 1991, *Molec. Crystals liq. Crystals*, **198,** 91.
[7] DEMIKHOV, E. I., DOLGANOV, V. K., and FILEV, V. M., 1983, *Soviet Phys. JETP Lett.*, **37,** 361.
[8] CHANDANI, A. D. L., HAGIWARA, T., SUZUKI, Y., OUCHI, Y., TAKEZOE, H., and FUKUDA, A., 1988, *Jap. J. appl. Phys.*, **27,** L729.
[9] LI, J., TAKEZOE, H., and FUKUDA, A., 1991, *Jap. J. appl. Phys.*, **30,** 532.
[10] SAEVA, F. D., 1979, *Liquid Crystals—The Fourth State of Matter* (Marcel Dekker), Chap. 6.
[11] SACKMANN, E., and VOSS, J., 1972, *Chem. Phys. Lett.*, **14,** 528.
[12] LEE, J., OUCHI, Y., TAKEZOE, H., FUKUDA, A., and WATANABE, J., 1990, *J. Phys.: Condens. Matter*, **2,** SA271.
[13] DE VRIES, H., 1951, *Acta crystallogr.*, **4,** 219.
[14] ISOZAKI, T., FUJIKAWA, T., TAKEZOE, H., FUKUDA, A., HAGIWARA, T., SUZUKI, Y., and KAWAMURA, I., 1992, *Jap. J. appl. Phys.*, **31,** L1435.
[15] ISOZAKI, T., FUJIKAWA, T., TAKEZOE, H., FUKUDA, A., HAGIWARA, T., SUZUKI, Y., and KAWAMURA, I., 1993, *Phys. Rev.* B, **31,** 13439.
[16] TAKANISHI, Y., HIRAOKA, K., AGRAWAL, V. K., TAKEZOE, H., FUKUDA, A., and MATSUSHITA, M., 1991, *Jap. J. appl. Phys.*, **30,** 2023.
[17] HIRAOKA, K., TAKINISHI, Y., SKARP, K., TAKEZOE, H., and FUKUDA, A., 1991, *Jap. J. appl. Phys.*, **30,** L1819.
[18] ISOZAKI, T., HIRAOKA, K., TAKANISHI, Y., SKARP, K., TAKEZOE, H., FUKUDA, A., SUZUKI, Y., and KAWAMURA, I., 1991, *Liq. Crystals*, **12,** 59.
[19] KLEVENS, H. B., and PLATT, J. R., 1949, *J. chem. Phys.*, **17,** 470.
[20] BRAUD, E. A., 1945, *A. Rep. Progr. Chem.*, **42,** 105.
[21] LI, J., TAKEZOE, H., and FUKUDA, A., 1991, *Jap. J. appl. Phys.*, **30,** 532.
[22] IKEDA, A., TAKANISHI, T., TAKEZOE, H., FUKUDA, A., INUI, S., KAWANO, S., SAITO, M., and IWANE, H., 1991, *Jap. J. appl. Phys.*, **30,** L1032.
[23] YANG, C. C., 1972, *Phys. Rev. Lett.*, **28,** 955.
[24] SUZUKI, A., ORIHARA, H., ISHIBASHI, Y., YAMADA, Y., YAMAMOTO, N., MORI, K., NAKAMURA, K., SUZUKI, Y., HAGIWARA, T., KAWAMURA, I., and FUKUI, M., 1990, *Jap. J. appl. Phys.*, **29,** L336.
[25] INUI, S., KAWANO, S., SAITO, M., IWANE, H., TAKANISHI, Y., HIRAOKA, K., OUCHI, Y., TAKEZOE, H., and FUKUDA, A., 1990, *Jap. J. appl. Phys.*, **29,** L987.
[26] GOUDA, F., SKARP, K., and LAGERWALL, S. T., 1991, *Ferroelectrics*, **113,** 165.
[27] BLINC, R., COPIC, M., DREVENSEK, I., LEVSTIK, A., and MUSEVIC, I., 1991, *Ferroelectrics*, **113,** 59.
[28] FUJIKAWA, T., ORIHARA, H., ISHIBASHI, Y., YAMADA, Y., YAMAMOTO, N., MORI, K., NAKAMURA, Y., HAGIWARA, T., and KAWAMURA, I., 1991, *Jap. J. appl. Phys.*, **30,** 2826.
[29] ORIHARA, H., FUJIKAWA, T., ISHIBASHI, Y., YAMADA, Y., YAMAMOTO, N., MORI, K., NAKAMURA, K., SUZUKI, Y., HAGIWARA, T., and KAWAMURA, I., 1990, *Jap. J. appl. Phys.*, **29,** L333.